Monoenergetic-Proton-Radiography Measurements of Implosion Dynamics in Direct-Drive Inertial-Confinement Fusion

C. K. Li, F. H. Séguin, J. R. Rygg, J. A. Frenje, M. Manuel, and R. D. Petrasso

Plasma Science and Fusion Center, Massachusetts Institute of Technology, Cambridge, Massachusetts 02139, USA

R. Betti,* J. Delettrez, J. P. Knauer, F. Marshall, D. D. Meyerhofer,* D. Shvarts,† V. A. Smalyuk, and C. Stoeckl

Laboratory for Laser Energetics, University of Rochester, Rochester, New York 14623, USA

O. L. Landen and R. P. J. Town

Lawrence Livermore National Laboratory, Livermore, California 94550 USA

C. A. Back and J. D. Kilkenny

General Atomics, San Diego, California, 92186 USA
(Received 23 December 2007; published 2 June 2008)

Time-gated, monoenergetic radiography with 15-MeV protons provides unique measurements of implosion dynamics in direct-drive inertial-confinement fusion. Images obtained during acceleration, coasting, deceleration, and stagnation display a comprehensive picture of spherical implosions. Critical information inferred from such images, hitherto unavailable, characterizes the spatial structure and temporal evolution of self-generated fields and plasma areal density. Results include the first observation of a radial electric field inside the imploding capsule. It is initially directed inward (at $\sim 10^9$ V/m), eventually reverses direction ($\sim 10^8$ V/m), and is the probable consequence of the evolution of the electron pressure gradient.

The goal of inertial-confinement fusion (ICF) is ignition and high gain [1], which require that a cryogenic deuterium-tritium (DT) spherical capsule be symmetrically imploded. This implosion results in a small mass of low density, hot fuel at the center, surrounded by a larger mass of high density, low temperature fuel [1]. Shock coalescence ignites the hot spot, and a self-sustaining burn wave subsequently propagates into the main fuel region. In the direct-drive approach to ICF, such an implosion occurs in response to a large number of high-power, individual laser beams illuminating the surface of a capsule. Understanding and controlling implosion dynamics is essential for ensuring success [1].

Implosion dynamics have been studied experimentally with a number of diagnostics, including x-ray imaging [1–3], fusion-product spectrometry [4], and fusion-product imaging [5,6], but none of these provide a complete picture of the time evolution of mass assembly and self-generated electric (E) and magnetic (B) fields.

In this Letter we present new nuclear observations of implosion dynamics for direct-drive spherical capsules on the OMEGA laser facility [7], using monoenergetic proton radiography [8,9]. The combination of characteristics in our approach allows us to first, probe distributions of self-generated $E + B$ fields, second, determine ρR by measuring the energy loss of backlighting protons, and third, sample all the implosion phases from acceleration, through coasting and deceleration, to final stagnation, to provide a more comprehensive picture of ICF spherical implosions. The result is the first use of proton radiography to study

ICF implosion dynamics. We note that earlier work by Mackinnon *et al.* [10] successfully demonstrated the feasibility of imaging implosions with protons (produced, in their case, by laser-plasma interactions), backlighting plastic (CH) capsules that were imploded by six 1-μm-wavelength laser beams [11]. Most importantly as regards this Letter, they did not observe any evidence of radial electric fields of the sort reported here. This is probably due to the fact that their implosions were totally different from ours [11,12].

Our experiment is illustrated schematically in Fig. 1. An imaged CH capsule had an 860-μm initial diameter, 20-μm thick shell and 15-atm H_2 gas fill. It was imploded through direct drive with 40 beams of 0.35-μm UV laser light. The laser pulse was square, with a duration of 1-ns
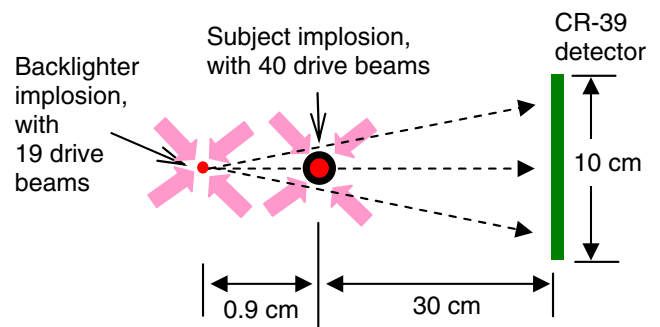

FIG. 1 (color online). Experimental setup, with proton backlighter, subject implosion, CR-39 imaging detectors, and laser beams. The field of view at the subject is ~3 mm.

and a total energy of ~16 kJ. Individual laser beams were smoothed using a single-color cycle, 1 THz two-dimensional (2D) smoothing by spectral dispersion (SSD), and polarization smoothing (PS) [13,14]. Implosions were backlit with monoenergetic protons (15.1 MeV) generated from D^3He-filled, exploding-pusher implosions driven by 19 laser beams [8,9]. The backlighting duration was ~130 ps, and the relative timing of backlighter and subject implosions was adjusted in each experiment so the proton radiograph would reflect the condition of the subject capsule at a desired time during its implosion. The effective FWHM of the backlighter is ≈ 40 μm [8], and this is the primary limit on the intrinsic spatial resolution of the imaging system. In images of imploded capsules, spatial resolution is degraded somewhat by scattering of imaging protons as they pass through the capsules [15,16].

Figure 2 shows a time sequence of proton radiographs covering the complete ICF implosion process from beginning through peak compression (each image from a different, but equivalent, implosion). The CR-39 detectors record the position and energy of every individual proton, so each radiograph can be displayed in two different ways: proton fluence vs position [Fig. 2(a)] or mean proton energy vs position [Fig. 2(b)]. In the uncompressed case (0.0 ns) the protons that passed through the shell limb lost the most energy, resulting in the dark ring of part (b), and were scattered the most, resulting in the light ring of part (a) (indicating low fluence at the detector). The images for later times provide important information about field distributions and capsule compression.

A striking feature of Fig. 2(a), indicating the presence of a time-varying radial electric field, is that a strong central peak appears in the fluence images during the early stages of implosion ($t = 0.8$–1.4 ns) while a strong central dip appears at later times ($t = 1.6$–2.1 ns) [17]. This is shown quantitatively in the radial line outs of Fig. 3. As we discuss

below, these features cannot be accounted for as a consequence of scatter. They must therefore result from the deflection of proton trajectories by radial electric fields. At early times the field must have been centrally directed in order to focus the protons passing within the capsule shell toward the center of the imaging detector. (Furthermore, for a smaller data set involving 36-beam cone-in-shell implosions, and for only a single time during the coasting phase, we observed this same focusing effect [18].) To account for the rapid change from a central fluence peak to a central fluence dip at ~1.5 ns, the radial field must have either reversed direction or suddenly become at least 3 times larger at that time (as shown by Monte Carlo simulations), in which case all protons would strike the detector outside the shadow of the capsule.

Because of the importance of these conclusions, it is important to rule out scattering as the cause of the central peak and central dip of Fig. 3. For the earlier times, simulations show that Coulomb scattering angles are not large enough to deflect protons to the image center. For the later times, Monte Carlo simulations indicate that proton scattering can reduce the central proton fluence by ~30% relative to values outside the capsule, but reductions in the actual images are ~90%. In both cases, we conclude that scatter cannot be the dominant mechanism.

The E-field source that is consistent with the data is the gradient of plasma electron pressure ($E \approx -\nabla p_e/en_e$) [19] (other possible sources do not fit as naturally with the data [20]). The pressure gradient has the correct sign at early times, and it reverses direction at about the correct time. This is illustrated in the p_e and n_e profiles at 0.8 and 1.9 ns, calculated by the LILAC hydrodynamic code [21] and shown in Fig. 4. Using calculated ∇p_e and n_e at different times, we estimate the strengths of E as varying
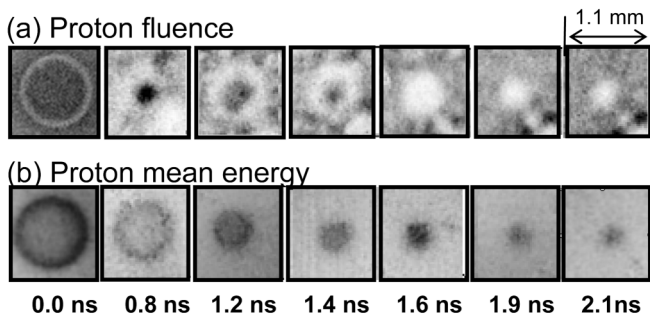

FIG. 2. 15.1-MeV proton radiographs of imploding capsules at different times, illustrating the time evolution of mass distribution and of a previously unobserved radial electric field. In the fluence images (a), darker means higher fluence, while in the energy images (b) darker means lower proton energy (more matter traversed). The gray-scale mapping is different for each image, to account for different backlighter yields (see Fig. 3) and make the most important structure clearly visible.
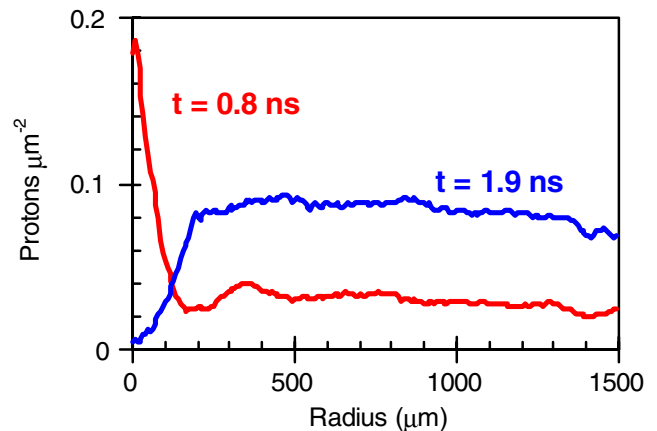

FIG. 3 (color online). Radial profiles of two proton fluence images of Fig. 2, showing the strong central peak at $t = 0.8$ ns and the strong central dip at 1.9 ns that can only be plausibly explained as being due to radial electric fields in the capsules, not by scattering of the imaging protons. The profiles are averaged over azimuthal angle, excluding the stalk region. The difference in fluence levels outside the two capsules is due to the difference in the backlighter proton yields.
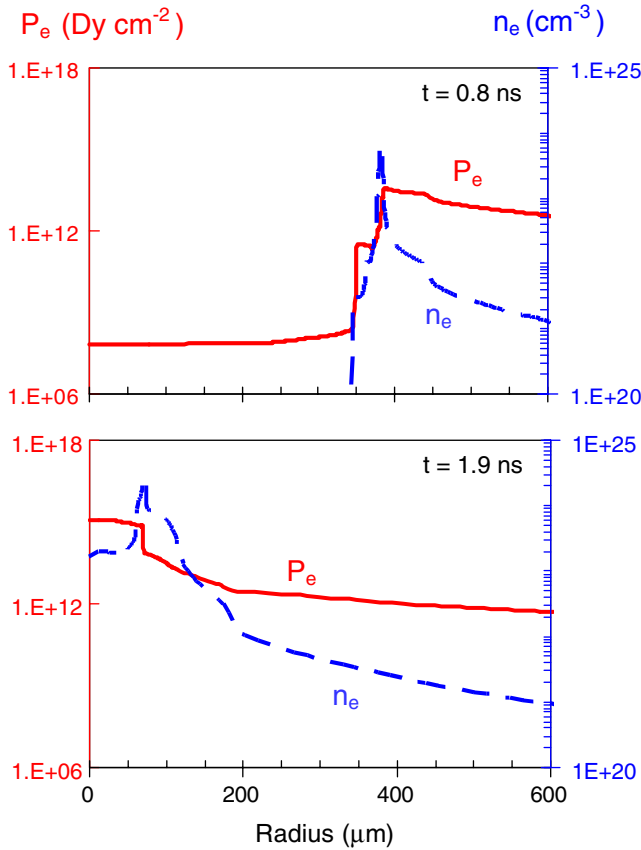
FIG. 4 (color online).   Profiles of electron pressure (solid lines) and density (dashed lines) at 0.8 and 1.9 ns, calculated by LILAC.
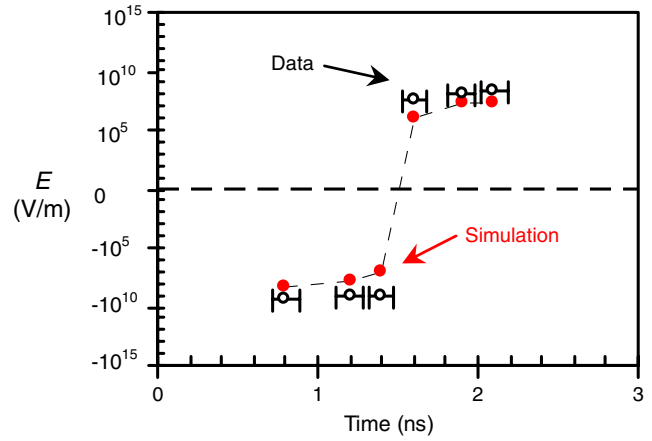

FIG. 5 (color online).   Radial E fields estimated from experimental measurements (open circles) and from LILAC simulations (solid circles) vs implosions times. Horizontal error bars represent uncertainties in backlighter burn time. Vertical error bars are about the size of the symbols.

and larger values of ρR, than measured at the times of nuclear burn (~ 1.9 ns) and peak compression (~ 2.1 ns). This indicates that the implosions had approximately 1D performance, with little impact from hydrodynamic instabilities, before deceleration. It has been suggested that performance approaches 1D because of full single-beam
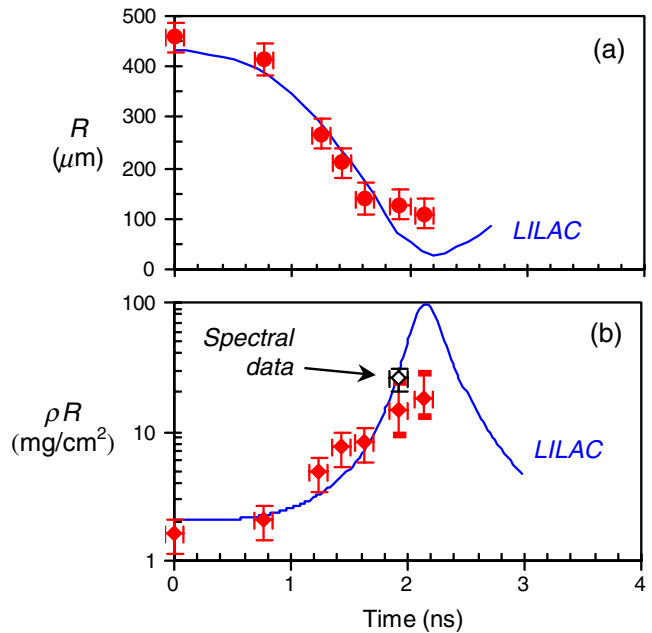
from $\sim -10^9$ to $\sim 10^8$ V/m (Fig. 5). Figure 5 also shows experimental field values deduced from the data of Fig. 2(a) [22]. The predictions corroborate the data in three crucial ways: the field strength and sign before the reversal ($\sim -10^9$ V/m, directed inward), the time of the field reversal (~ 1.5 ns), and the field strength after the reversal ($\sim 10^8$ V/m directed outward). Furthermore, simulations of image formation show that only if the effects of the fields are added to the effects of scattering can the peaks and dips of the simulations plausibly match the data. This match leads to a high level of confidence that ∇p_e is the probable source of the observed phenomena. Note that the detailed structures of the fluence images are also modified, in ways that do not affect our conclusions, by the in-flight movement of the shell ($V_{\rm imp} \sim -2.5 \times 10^7$ cm/s), which is ~ 30 μm during the backlighter burn time (~ 130 ps.)

Quantitative information about capsule sizes and ρRs at different times is extracted from line outs through the images in Fig. 2(b); the mean width provides the average capsule size ($\approx 2R$), while the mean height indicates the total ρL ($\approx 2 \times \rho R$). The data are contrasted with LILAC simulations in Fig. 6; the simulations come reasonably close to matching the observed evolution of capsule convergence and ρR during the acceleration and coasting phases (~ 0–1.6 ns), but predict smaller values of radius,

FIG. 6 (color online).   Measured capsule radii [solid circles, (a)] and ρR [solid diamonds (b)] compared with LILAC 1D simulations (solid lines). Horizontal error bars represent uncertainties in backlighter burn time. The open diamond point in (b) represents the ρR of a comparable implosion of a D^3He-filled capsule at bang time, measured by several proton spectrometers in different directions; this completely different type of measurement is statistically consistent with the data derived here from radiography images.

PHYSICAL REVIEW LETTERS

smoothing, which significantly improves the shell integrity during the acceleration phase, and because thickening of the shell during subsequent coasting further enhances shell integrity [14]. The apparent degradation of capsule performance at later times relative to the 1D simulation could be largely a consequence of fuel-shell mixing [23] and implosion asymmetry [24].

It is worthwhile to compare these measured ρR values with a value obtained using a completely different method during an equivalent implosion. The open black data point in Fig. 6(b) was obtained by using proton spectrometry to determine the energy of self-emitted D^3He protons; the downshift in the energy of these protons implies a ρR [25] at bang time of ~ 25 mg/cm^2. This is slightly higher than the measurement made here, but statistically consistent with it. On the other hand, the spectrometry-implied value is closer to the 1D value, which raises the possibility that the radiography-implied value loses accuracy when the capsule becomes sufficiently compressed that images are noticeably affected by proton scatter. This is currently being investigated.

Finally, the residual mass during the implosion can be estimated in terms of the measured R [Fig. 6(a)] and measured ρR [Fig. 6(b)]: $m/m_0 \approx C_r^{-2} \rho R(t)/\rho R(0)$, where $C_r \equiv R(0)/R(t)$ is the target convergence ratio. This indicates that $\sim(30$–$40)\%$ of the shell has been ablated by bang time. Although the mass estimates have large uncertainties due to those associated with both R and ρR measurements, they are helpful for illustrating the dynamics of mass ablation during implosions.

In summary, new observations and measurements of direct-drive spherical implosions have been made with monoenergetic proton radiography. Quantitative information inferred from proton images characterizes the spatial structure and temporal evolution of an imploding capsule, dynamically displaying a comprehensive picture of direct-drive ICF implosions. The observations include the first experimental evidence of radial E fields inside implosion capsules, their reversal in direction, and their plausible connection with plasma pressure gradients.

---

*Also at Department of Mechanics Engineering, Physics and Astronomy, University of Rochester, Rochester, NY 14623, USA.

†Also at NRCN, Negev and Ben Gurion University of the Negev, Beer-Sheva 84015, Israel.

[1] S. Atzeni and J. Meyer-Ter-Vehn, *The Physics of Inertial Fusion* (Clarendon Press, Oxford, 2004).

[2] F. J. Marshall *et al.*, Phys. Plasmas **11**, 251 (2004).

[3] R. S. Craxton *et al.*, Phys. Plasmas **12**, 056304 (2005).

[4] F. H. Séguin *et al.*, Rev. Sci. Instrum. **74**, 975 (2003).

[5] L. Disdier *et al.*, Phys. Plasmas **13**, 056317 (2006).

[6] F. H. Séguin *et al.*, Rev. Sci. Instrum. **75**, 3520 (2004).

[7] J. M. Soures *et al.*, Phys. Plasmas **3**, 2108 (1996).

[8] C. K. Li *et al.*, Rev. Sci. Instrum. **77**, 10E725 (2006).

[9] C. K. Li *et al.*, Phys. Rev. Lett. **97**, 135003 (2006).

[10] A. Mackinnon *et al.*, Phys. Rev. Lett. **97**, 045001 (2006).

[11] The images of Ref. [10] show no evidence of fields in or near the capsule, in contrast to our observations. The difference is probably attributable to completely different implosion conditions, and the fact that there were timing inconsistencies between their beams [12]. Their proton backlighter was also very different, with a lower energy (5–7 MeV) and broader spectrum.

[12] A. Mackinnon (private communication).

[13] S. Skupsky *et al.*, Phys. Plasmas **6**, 2157 (1999).

[14] D. D. Meyerhofer *et al.*, Phys. Plasmas **8**, 2251 (2001).

[15] V. L. Highland, Nucl. Instrum. Methods **129**, 497 (1975).

[16] A simple analytic model [15] can be used to estimate the characteristic scattering angle in radians for protons passing through a plasma with areal density ρL: $\langle \theta_{sc} \rangle = z(15 \text{ MeV}/p\beta c)(\rho L/\rho L_{rad})^{1/2}$, where $z = 1$ for protons; $p\beta c = 30$ MeV for 15 MeV protons; $\rho L_{rad} = 4.34 \times 10^4$ mg/cm^2 for carbon. For example, if $\rho L \approx 20$ mg/cm^2, then $\langle \theta_{sc} \rangle \sim 0.6°$.

[17] Monte Carlo simulations of the imaging system show that, for a given amount of deflection, the character of focusing or defocusing in the image is insensitive to the specific distance of the detector position.

[18] J. R. Rygg *et al.*, Science **319**, 1223 (2008).

[19] S. I. Braginskii, *Review of Plasma Physics* (Consultants Bureau, New York, 1965).

[20] For example, the contribution of charge separation around the convergent shock front due to the imbalance of ion mean-free paths between the shocked and unshocked plasmas will neither reverse direction nor suddenly increase as the data require. (We have ignored contributions from the outgoing shock front at later times due to its relatively weaker strength.)

[21] J. A. Delettrez *et al.*, Phys. Rev. A **36**, 3926 (1987).

[22] The electric field E was derived from the images by using $E \sim 2\xi\varepsilon_p(A + a)(eAaL)^{-1}$, where $\varepsilon_p = 15$ MeV is the proton energy, e is electron charge, $a = 0.9$ cm and $A = 30.9$ cm are distances from backlighter to implosion and from backlighter to detector, respectively, $|\xi| \sim (0.5$–$1)R$ is the apparent displacement of protons in the subject plane due to the effects of E on the proton trajectories, and $L \sim (0.5$–$2)R$ is the proton path length.

[23] C. K. Li *et al.*, Phys. Rev. Lett. **89**, 165002 (2002).

[24] C. K. Li *et al.*, Phys. Rev. Lett. **92**, 205001 (2004).

[25] C. K. Li and R. D. Petrasso, Phys. Rev. Lett. **70**, 3059 (1993).